The HKU Scholars Hub The University of Hong Kong 香港大學學術庫

Title	Dynamic Prediction of Correlated Color Temperature and Color Rendering Index of Phosphor-Coated White Light-Emitting Diodes
Author(s)	Chen, H; Hui, SYR
Citation	IEEE Transactions on Industrial Electronics, 2014, v. 61 n. 2, p. 784-797
Issued Date	2014
URL	http://hdl.handle.net/10722/189056
Rights	©2014 IEEE. Personal use of this material is permitted. However, permission to reprint/republish this material for advertising or promotional purposes or for creating new collective works for resale or redistribution to servers or lists, or to reuse any copyrighted component of this work in other works must be obtained from the IEEE

Dynamic Prediction of Correlated Color Temperature and Color Rendering Index of Phosphor-Coated White Light-Emitting Diodes

Huanting Chen and S. Y. (Ron) Hui, *Fellow, IEEE*

***Abstract*—Light-emitting diode (LED) technology is a multidisciplinary subject that involves photometry, electric power, heat, and chromaticity which are interdependent on one another. So far, the photoelectrothermal (PET) theory has linked up the first three aspects. This research includes chromaticity into the dynamic PET theory so that even the correlated color temperature (CCT) and color rendering index (CRI) of phosphor-coated white LEDs can be dynamically predicted, thus overcoming the low bandwidth problem of some light measurement equipment. This dynamic modeling of CCT and CRI has been verified with favorable agreements between theoretical predictions and measurements of several LED samples. The outcome of this project offers a new research and development tool for practicing LED system designers to predict the instantaneous variations of CCT and CRI when the power varies in a LED system.**

***Index Terms*—Chromaticity, color rendering index (CRI), correlated color temperature (CCT), light-emitting diodes (LEDs), spectral power distribution (SPD).**

NOMENCLATURE

P_λ	Spectral power distribution (SPD) (mW/nm).
h	Planck's constant (J · s).
c	Speed of light (m · s^{-1}).
λ	Wavelength (nm).
E_g	Bandgap energy (eV).
k	Boltzmann constant (J · K^{-1}).
T	Carrier temperature (°C).
$P_{\rm opt}$	Optical power (W).
T_j	Junction temperature (°C).
$\lambda_{\rm peak}$	Peak wavelength (nm).
$\Delta\lambda$	Full-width at half-maximum (FWHM) (nm).
η	Ratio of specific spectra to white spectrum, dimensionless.
η_w	Wall-plug efficiency, dimensionless.
R	Thermal resistance (°C/W).
C	Thermal capacitance (J/°C).
t	Time variable.
$P_{\rm opt\_b}$, $P_{\rm opt\_g}$, $P_{\rm opt\_y}$, and $P_{\rm opt\_total}$	Optical power (W) for the blue, green, yellow, and white spectra, respectively.
$\lambda_{\rm peak\_b}$, $\lambda_{\rm peak\_g}$, and $\lambda_{\rm peak\_y}$	Peak wavelengths (nm) for the blue, green, and yellow spectra, respectively.
σ_b, σ_g, and σ_y	FWHM-related coefficients (nm) for the blue, green, and yellow spectra, respectively.
η_b, η_g, and η_y	Ratios of blue–green–yellow (B–G–Y) spectra to white spectrum, respectively, dimensionless.
λ_1, λ_2	Wavelengths at half of the peak intensity.
P_d	Light-emitting diode (LED) power (W).
k_h	Heat dissipation coefficient of LED device, dimensionless.
T_0	Ambient or rated reference temperature (25 °C).

Manuscript received September 3, 2012; revised January 19, 2013; accepted February 10, 2013. Date of publication March 7, 2013; date of current version August 9, 2013. This work was supported by the Hong Kong Research Grant Council under Theme-based Research Project T22-715-12N.

H. Chen is with the Department of Electrical and Electronic Engineering, The University of Hong Kong, Hong Kong (e-mail: htchen23@gmail.com).

S. Y. Hui is with the Department of Electrical and Electronic Engineering, The University of Hong Kong, Hong Kong, and also with Imperial College London, London, SW7 2AZ, U.K. (e-mail: r.hui@imperial.ac.uk; ronhui@eee.hku.hk).

Color versions of one or more of the figures in this paper are available online at http://ieeexplore.ieee.org.

Digital Object Identifier 10.1109/TIE.2013.2251736

I. INTRODUCTION

IN THE last two decades, the light-emitting diode (LED) technology has been commercially adopted in display, decorating, and signaling applications and, to some extent, also in general lighting. For some lighting applications, such as in textile industry, offices, hotels, and galleries, the correlated color temperature (CCT) and the color rendering index (CRI) are important factors in the choice of light sources. The CRI is presently the only internationally accepted metric for assessing the color-rendering performance of light sources, although reviews have been conducted recently to examine other means to quantify color rendering [1], [2] in view of the spectral characteristics of the emerging LED technology. Several reports [3]–[5] have pointed out that the CCT of the phosphor-coated white LED will change with the LED power. The influence of the junction temperature on chromaticity and color-rendering properties of trichromatic white-light sources based on LEDs has been studied [6], and the relationships of the light spectra of the LEDs and the junction temperature have also been practically observed [7], [8]. The spectral power distribution (SPD) of LED is therefore an important characteristic that determines the optical power, luminous flux, and color properties. Such an SPD depends on electrical power and the junction temperature. However, the electrothermal dependence for SPD is often not

0278-0046 © 2013 IEEE

precisely characterized in the device data sheets. It is difficult to describe the SPD qualitatively from the data sheet information without the help of a spectrometer.

LEDs emit light through the spontaneous recombination of electron–hole pairs and simultaneous emission of photons. In theory, the SPD of LED is proportional to the product of the Boltzmann distribution and density of states, which can be expressed as

$$P_\lambda \propto \sqrt{\frac{hc}{\lambda} - E_g} \exp\left(-\frac{hc}{\lambda kT}\right). \quad (1)$$

However, (1) has not included all semiconductor physical factors of LED, leading to significant deviation between the theoretical and practical SPDs in a previous study [9]. The SPD modeling of LED based on Gaussian functions, which includes only the physical parameter of peak wavelength, has been proposed in [10]. Extended Gaussian functions using other physical parameters such as optical power and Stokes energy loss have also been considered [6]. In addition, the Gaussian model has been extended with the use of double functions [11], [12], which are nowadays still used for lighting calculations by the International Commission on Illumination (CIE). The dependence of the SPD of LED on temperature and current was reported in [7] and [13]. However, LED application engineers, who usually have electronic engineering backgrounds, tend to lack the required light science knowledge which is essential in the optimal design of LED systems. So far, there is a lack of theory linking all the essential factors for LED system optimization.

The general photoelectrothermal (PET) theory for LED systems [14] has linked up the interactions of heat, luminous flux, and power in LED systems, which aims at providing a comprehensive LED system theory with physical explanations for electronics engineers and researchers working in LED system designs [15]. However, there is a lack of LED system theory that can incorporate the variation of the CCT and CRI with power variation. In this paper, a spectral model based on the steady-state and dynamic PET theory [16] is proposed to describe the color properties of phosphor-coated white LEDs (blue LED and yellow phosphor coating) under steady and transient operations. This novel model is intended to incorporate the following important physical parameters together in an integrated manner:

1) electric parameters: power and current;
2) optical and spectral parameters: optical power, peak wavelength, and FWHM;
3) thermal parameters: junction temperature and heat sink temperature;
4) device parameters: thermal resistance and thermal capacitance;
5) time.

A distinctive feature of the proposed method is that the model parameters are extracted from the steady-state tests only while the modeling can be applied to both steady-state and dynamic situations. It is envisaged that this model is the first of its kind that can be used by phosphor-coated white LED system designers to establish the spectral model and then evaluate the variations of the CCT and CRI. So far, there is no systematic R&D tool that can predict the instantaneous variations of the CCT and CRI. This research project aims at filling this theoretical gap by relating the variation of the CCT and CRI to the phosphor-coated white LED system power. The proposed theory has been tested successfully with practical measurements based on several LED samples.

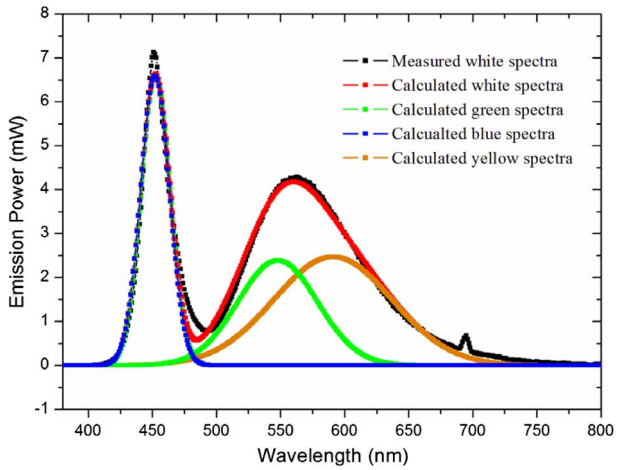

Fig. 1. Measured and calculated SPDs for Sharp 4.4-W LED at a junction temperature of 68.6 °C and a current of 0.34 A.

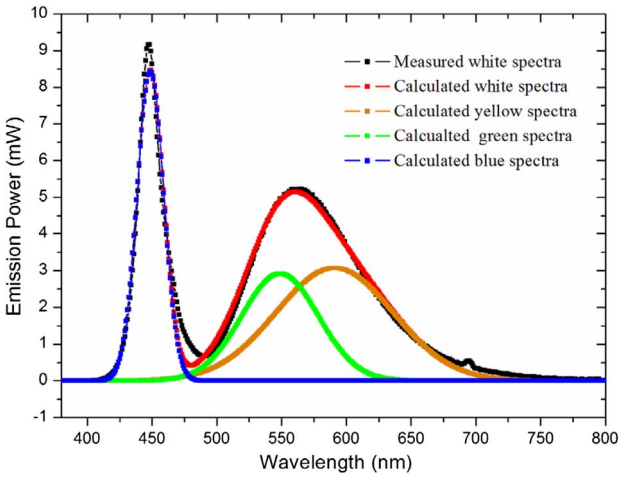

Fig. 2. Measured and calculated SPDs for Sharp 8-W LED at a junction temperature of 66.3 °C and a current of 0.34 A.

II. SPD Modeling and Practical Measurement Methods

A. SPD of YAG Phosphor-Coated White LED

The asymmetrical SPD of monochrome LED is typically modeled with Gaussian function [6]

$$P_\lambda = P_{\text{opt}} \frac{1}{\sigma\sqrt{2\pi}} \exp\left[-0.5^* \frac{(\lambda - \lambda_{\text{peak}})^2}{\sigma^2}\right] \quad (2)$$

where σ is dependent on peak wavelength λ_{peak} and FWHM $\Delta\lambda$ can be expressed as

$$\sigma = \frac{\lambda_{\text{peak}}^2 \Delta E}{2hc\sqrt{2\ln 2}} = \frac{\lambda_{\text{peak}}^2 \left(\frac{hc}{\lambda_1} - \frac{hc}{\lambda_2}\right)}{2hc\sqrt{2\ln 2}} = \frac{\lambda_{\text{peak}}^2 \left(\frac{hc\Delta\lambda}{\lambda_1\lambda_2}\right)}{2hc\sqrt{2\ln 2}}. \quad (3)$$

TABLE I
MEASURED SPECTRUM AND FITTING PARAMETERS RELATED TO TRIPLE-COLOR MODELING OF LED SAMPLES

	P_{opt_b} (W)	P_{opt_g} (W)	P_{opt_y} (W)	λ_{peak_b} (nm)	λ_{peak_g} (nm)	λ_{peak_y} (nm)	σ_b (nm)	σ_g (nm)	σ_y (nm)
Sharp 4.4W (T_j:84.5°C,P_d:3.4W)	0.187	0.185	0.284	452.8	548.0	591.0	22.6	62.0	91.9
Sharp 8W (T_j:66.9°C,P_d:3.2W)	0.218	0.216	0.348	448.7	549.0	591.0	20.6	59.1	90.2

The SPD of a white LED using yellow YAG phosphor and blue LED chip can theoretically be considered as the sum of the blue and yellow spectra. In practice, however, the so-called yellow phosphor emits light in both of the yellow and green spectra (as indicated from the measured spectra in Figs. 1 and 2). If a blue and a yellow spectrum are chosen, the difference between the practically measured SPD and double-color (blue and yellow color) spectrum model can be represented by a green spectrum. Therefore, in order to represent the practical situation, a green spectrum can be added to the double-spectrum model, resulting in the following analytical trispectrum (B–G–Y) model described by (4) and subsequently modified as (5):

$$\begin{aligned} P_\lambda = {} & P_{\text{opt\_b}} \frac{1}{\sigma_b\sqrt{2\pi}} \exp\left[-0.5^* \frac{(\lambda-\lambda_{\text{peak\_b}})^2}{\sigma_b^2}\right] \\ & + P_{\text{opt\_g}} \frac{1}{\sigma_g\sqrt{2\pi}} \exp\left[-0.5^* \frac{(\lambda-\lambda_{\text{peak\_g}})^2}{\sigma_g^2}\right] \\ & + P_{\text{opt\_y}} \frac{1}{\sigma_y\sqrt{2\pi}} \exp\left[-0.5^* \frac{(\lambda-\lambda_{\text{peak\_y}})^2}{\sigma_y^2}\right] \end{aligned} \quad (4)$$

$$\begin{aligned} P_\lambda = {} & \eta_b P_{\text{opt\_total}} \frac{1}{\sigma_b\sqrt{2\pi}} \exp\left[-0.5^* \frac{(\lambda-\lambda_{\text{peak\_b}})^2}{\sigma_b^2}\right] \\ & + \eta_g P_{\text{opt\_total}} \frac{1}{\sigma_g\sqrt{2\pi}} \exp\left[-0.5^* \frac{(\lambda-\lambda_{\text{peak\_g}})^2}{\sigma_g^2}\right] \\ & + \eta_y P_{\text{opt\_total}} \frac{1}{\sigma_y\sqrt{2\pi}} \exp\left[-0.5^* \frac{(\lambda-\lambda_{\text{peak\_y}})^2}{\sigma_y^2}\right]. \end{aligned} \quad (5)$$

Therefore, the SPD modeling for the phosphor-coated white LED can be expressed as a tricolor spectrum, which can be considered as an extended Gaussian model.

B. Practical Spectral Power Modeling Process

The proposed spectral modeling process has been demonstrated with the use of the following: 1) Sharp 4.4-W LED (Model number: GW5BNC15L02) and 2) Sharp 8-W LED (Model number: GW5BWC15L00). The practical white spectra of the LED samples are first recorded. The parameters required for (4) can then be extracted from measured spectra based on standard curve-fitting numerical tool and are shown in Table I. Figs. 1 and 2 show the measured SPD and the corresponding theoretical tricolor spectra for the 4.4- and 8-W LED samples, respectively. For the Sharp LED samples, the phosphor is doped by a combination of YAG: Ce yellow phosphor and red phosphor (such as GaAlSiN3:Eu). The calculated results (red curve) agree well with practical measurements (black curve). These agreements confirm the validity of the proposed tricolor SPD modeling method.

C. Temperature Dependence of the Peak Wavelength and FWHM

1) For Blue LED Chip: The peak wavelength of the blue LED chip moves toward the shorter wavelength direction (i.e., blue shift) with increasing current at constant temperature [7]. This is due to the piezoelectricity-induced quantum-confined Stark effect. On the contrary, there is a red shift of the peak wavelength of the blue chip with an increasing temperature at constant current, which can be attributed to the variation in the semiconductor bandgap with temperature. For LED devices, this red shift of the wavelength due to the change of the bandgap energy has been described by the Varshni equation [21], which consists of curve-fitting coefficients [23]. The red- and blue-shift phenomena on different LED models have been observed independently by several research groups as parabolic functions in the relationships of the peak wavelength and junction temperature for a range of LED current (see [18, Fig. 1]) and the peak wavelength and driving current (see [22, Fig. 3]).

Because the driving current and the junction temperature of the LED are proportional to the LED power, the practical parabolic relationships observed in [18] and [22] can be generalized as a parabolic function of LED power as shown in (6).

The peak wavelength–electrical power curve for the blue LED can be divided into the blue- and red-shift regions. In the low electrical power range, the peak wavelength decreases approximately linearly with increasing electrical power to reflect the domination of the piezoelectricity-induced quantum-confined Stark effect. As the junction temperature increases with increasing electrical power, the temperature influence on the semiconductor energy gap starts to dominate, and the peak wavelength moves linearly toward longer wavelengths with increasing electrical power, which has been indicated in (8). Therefore, the electrical power dependence of the peak wavelength can be expressed as a parabolic function

$$\lambda_{\text{peak\_b}}(P_d, T_j) = a(T_j)P_d^2 - b(T_j)P_d + \beta_{\text{peak\_b}} \quad (6)$$

where $\beta_{\text{peak\_b}}$ is the referenced $\lambda_{\text{peak\_b}}$ peak wavelength of the blue spectrum at the ambient temperature T_0; a and b are positive coefficients dependent on the junction temperature.

It should be noted that (6) is only valid for the GaN-based LED because the peak wavelength for the AlGaInP LED is a linear function of the electrical power [18]. Additionally, this expression should apply to the junction temperature as a function of electrical power at constant ambient temperature. As P_d increases from a small value, λ_{peak} decreases almost linearly because the first positive term of (6) is negligible when P_d is small. As P_d continues to increase, the first positive term, which is proportional to the square of P_d, will increase λ_{peak} significantly. Consequently, the peak wavelength is expected

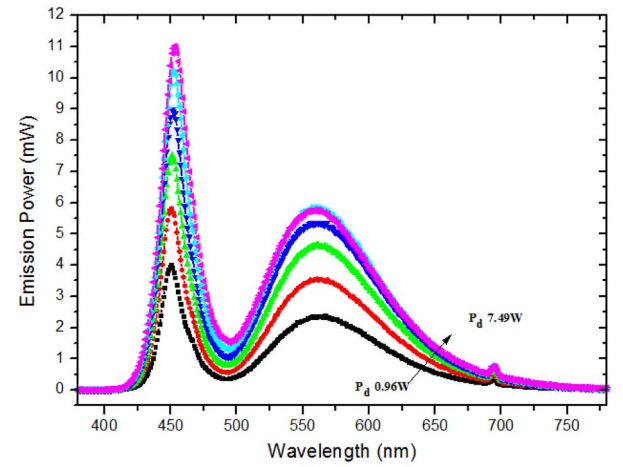

(a)

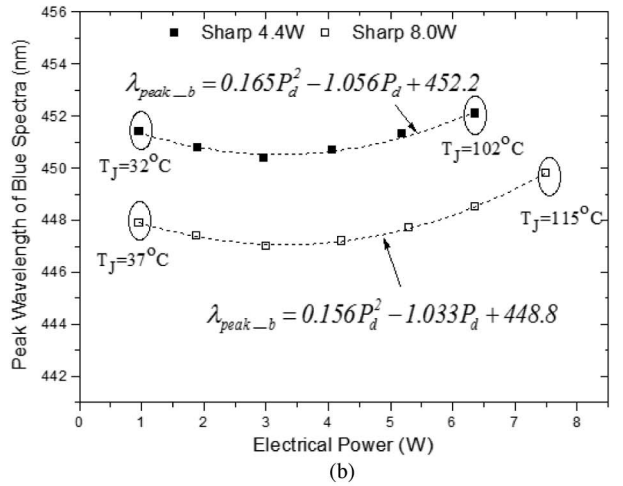

(b)

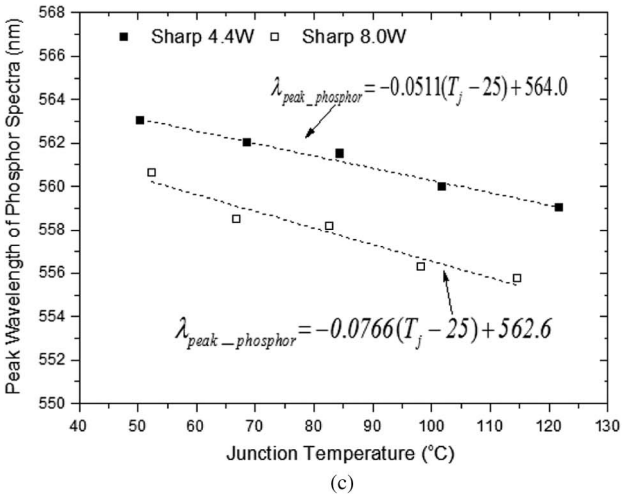

(c)

Fig. 3. (a) Measured SPDs for Sharp 4.4-W LED versus electrical power. (b) Measured peak wavelengths of blue spectra versus electrical power of Sharp 4.4- and 8-W LED samples. (c) Measured peak wavelengths of the phosphor spectra versus the junction temperature of Sharp 4.4- and 8-W LED samples.

to follow a parabolic curve with a minimum value. Starting from a referenced value at a reference electrical power P_{d0}, the position of the peak wavelength at any electrical power P_d can be calculated. As the peak wavelength of the blue LED chip varies with electrical power, the emission efficiency and wavelength for phosphor will also be influenced.

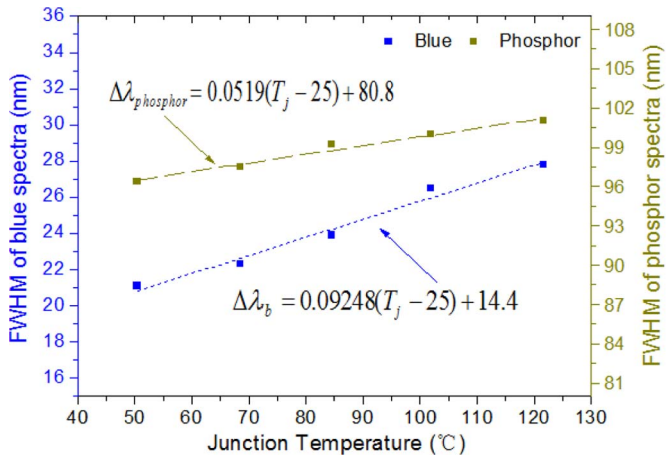

Fig. 4. Measured FWHM of blue and phosphor spectra versus junction temperature of Sharp 4.4-W LED.

To validate the theory, the Sharp 4.4-W LED sample is mounted on a heat sink with a thermal resistance of 8.3 °C/W for tests in the range of electrical power from 0. 68 to 6.4 W. The Sharp 8-W LED sample is mounted on a heat sink with a thermal resistance of 10.2 °C/W. Fig. 3(b) shows the variations of the peak wavelength of the blue spectra with electrical power for the Sharp 4.4- and 8-W samples. The two measured curves are found to be parabolic functions that can be described by (6). These results are consistent with the parabolic measurements reported in [18] and [22]. As shown in Fig. 3(a), the measured phosphor spectra clearly shift to shorter wavelengths with electrical power.

2) For Phosphor Coating: The measured peak wavelengths of the phosphor spectra as a function of the junction temperature for the two LED samples are included in Fig. 3(a) and (c), which have clearly shown decreasing peak wavelength of phosphor spectra with the junction temperature. The same physical observation has been reported in [24]. The data form two straight lines with negative slopes, which can be expressed by the linear equation

$$\lambda_{\text{peak\_phosphor}}(T_j) = k_{\text{peak\_phosphor}}(T_j - T_o) + \beta_{\text{peak\_phosphor}}. \quad (7)$$

The coefficients required for (6) and (7) can be extracted from the practical measurements as highlighted in Fig. 3(b) and (c).

The theoretical FWHM for the spectra is $1.25 \times 10^{-7}\lambda_{\text{peak}}^2 T_j$ [13], where T_j is the junction temperature in kelvin. However, the emission width is much higher than the theoretical value due to the composition inhomogeneity of the alloy used in the active layer. The FWHM for the spectra is broadened with the increasing temperature and can be modeled as

$$\Delta\lambda(T_j) = k_{\Delta\lambda}(T_j - T_0) + \beta_{\Delta\lambda} \quad (8)$$

where $k_{\Delta\lambda}$ is the slope value between junction temperature and FWHM and $\beta_{\Delta\lambda}$ is the referenced $\Delta\lambda$ FWHM at rated junction temperature T_0. The parameters required for (8) can be determined from Fig. 4.

TABLE II
MEASURED SPECTRUM AND FITTING PARAMETERS RELATED TO TEMPERATURE DEPENDENCE OF PEAK WAVELENGTHS AND FWHM FOR DIFFERENT TYPES OF LEDS

	a (nm/W²)	b (nm/W)	β_{peak_b} (nm)	$k_{peak\_phosphor}$ (nm/°C)	$\beta_{peak\_phosphor}$ (nm)	$k_{\Delta\lambda\_b}$ (nm/°C)	$\beta_{\Delta\lambda\_b}$ (nm)	$k_{\Delta\lambda\_phosphor}$ (nm/°C)	$\beta_{\Delta\lambda\_phosphor}$ (nm)
Sharp 4.4W	0.165	1.056	452.2	-0.0511	564.0	0.0925	14.4	0.0519	80.8
Sharp 8W	0.156	1.033	448.8	-0.0766	562.6	0.0589	15.4	0.0537	93.1

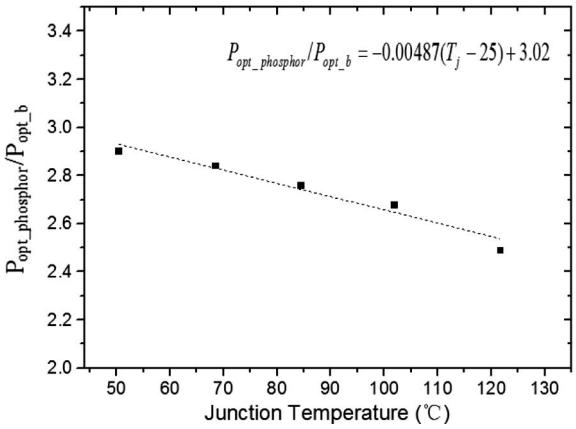

Fig. 5. Measured $P_{\rm opt\_phosphor}/P_{\rm opt\_b}$ ratio versus junction temperature of Sharp 4.4-W LED.

As shown in Figs. 3 and 4, the measured variations in the peak wavelength and FWHM exhibit approximately linear behavior with the junction temperature, which justifies the format of (8). For the different types of LEDs under consideration, the temperature coefficients of the peak wavelength and FWHM have been summarized in Table II.

D. Temperature Dependence of the $P_{\rm opt\_phosphor}/P_{\rm opt\_b}$ Ratio

The ratio between the optical power of the phosphor spectra and the optical power of the blue spectra is related to the junction temperature [18]. The ratio of $P_{\rm opt\_phosphor}/P_{\rm opt\_b}$ can be established as a function of the junction temperature using the practical measurement as shown in Fig. 5. This relationship can be expressed as

$$\frac{P_{\rm opt\_phosphor}}{P_{\rm opt\_b}}(T_j) = \frac{(1-\eta_b)P_{\rm opt\_total}}{\eta_b P_{\rm opt\_total}}(T_j) = k_{\rm opt}(T_j - T_0) + \beta_{\rm opt} \quad (9)$$

where $\beta_{\rm opt}$ is the referenced $P_{\rm opt\_phosphor}/P_{\rm opt\_b}$ ratio at the rated junction temperature T_0 and $k_{\rm opt}$ is the slope of the measured line of (9). The coefficients required for (9) can be obtained from the practical measurements as illustrated in Fig. 5. It is noted that $P_{\rm opt\_total}$ can be calculated under different junction temperature based on the PET theory [19]. Using (4)–(9), $P_{\rm opt\_b}$ can be determined with different junction temperature values. Therefore, the temperature and electrical power can be linked to the spectral modeling for white LED. The spectra of the LED samples have been measured at different junction temperature values, and the coefficients corresponding to (9) are tabulated in Table III. From the measurements, the ratios $P_{\rm opt\_g}/P_{\rm opt\_phosphor}$ and $P_{\rm opt\_y}/P_{\rm opt\_phosphor}$ can be assumed constant at different junction temperature values.

III. DETERMINATION OF JUNCTION TEMPERATURE, CCT, AND CRI USING THE DYNAMIC PET THEORY FRAMEWORK

A. Temperature and Electrical Power Dependence of the Optical Power

Based on the steady-state PET theory [14], [19], the relationship of the wall-plug efficiency (η_W) as a function of the junction temperature (T_j) for constant LED power (P_{d0}) operation is fairly linear and can be approximated as a linear relationship

$$\eta_W(T_j, P_{d0}) = \alpha T_j + \beta \quad (10)$$

where α is a coefficient representing the slope of the relationship and β is another coefficient. Both α and β can be obtained from the measurements in Fig. 6(a).

In practice, at constant junction temperature (T_{j0}), η_W can be obtained as a quadratic polynomial function of P_d

$$\eta_W(T_{j0}, P_d) = \chi P_d^2 + \delta P_d + \gamma \quad (11)$$

where χ, δ, and γ are constants that can be extracted from Fig. 6(b) with constant junction temperature. Based on the above analysis, η_W can be expressed as a link for P_d and T_j using a 2-D mathematical function as discussed in [19]. The function of η_W can be constructed as

$$\eta_W(T_j, P_d) = \frac{(\alpha T_j + \beta)\left(\chi P_d^2 + \delta P_d + \gamma\right)}{\mu} \quad (12)$$

where μ is the intersection value of function for (10) and (11), which is the value of η_W at point (T_{j0}, P_{d0}). Therefore, the optical power can be expressed as

$$P_{\rm opt}(T_j, P_d) = \eta_W P_d = \frac{(\alpha T_j + \beta)\left(\chi P_d^3 + \delta P_d^2 + \gamma P_d\right)}{\mu}. \quad (13)$$

As shown in Table IV, the parameters required for (13) can be extracted using the measured data.

TABLE III
MEASURED SPECTRUM AND FITTING PARAMETERS RELATED TO TEMPERATURE DEPENDENCE OF $P_{\mathrm{opt\_phosphor}}/P_{\mathrm{opt\_b}}$ FOR DIFFERENT TYPES OF LEDS

	k_{opt}	β_{opt}	$P_{opt\_g}/P_{opt\_phosphor}$	$P_{opt\_y}/P_{opt\_phosphor}$
Sharp 4.4W	-0.00487	3.02	0.327	0.673
Sharp 8W	-0.00602	3.05	0.309	0.691

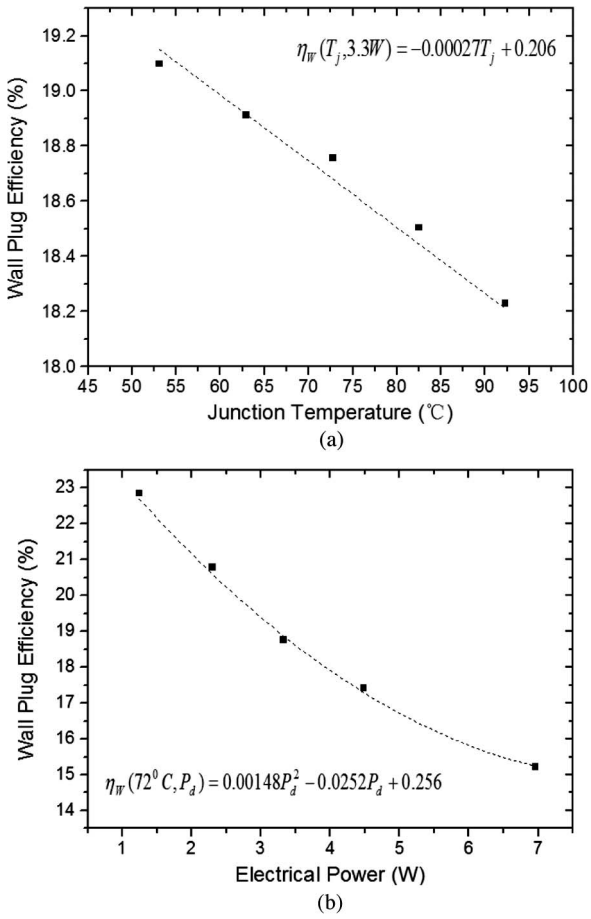

Fig. 6. (a) Measured wall-plug efficiency versus junction temperature of Sharp 4.4-W LED at constant electrical power. (b) Measured wall-plug efficiency versus electrical power of Sharp 4.4-W LED at constant junction temperature.

It should be noted that this spectral model in the PET theory framework can estimate the optical power of LED at any junction temperature and electrical power. Putting (6)–(9), and (13) into (5), the electrothermal SPD as a function of electrical power P_d and junction temperature T_j can be expressed as

$$P_\lambda(P_d,T_j) = \eta_b(T_j)P_{\mathrm{opt\_total}}(P_d,T_j)\frac{1}{\sigma_b(T_j)\sqrt{2\pi}} \times \exp\left\{-0.5^*\frac{[\lambda-\lambda_{\mathrm{peak\_b}}(P_d,T_j)]^2}{\sigma_b(T_j)^2}\right\} + \eta_g(T_j)P_{\mathrm{opt\_total}}(P_d,T_j)\frac{1}{\sigma_g(T_j)\sqrt{2\pi}} \times \exp\left\{-0.5^*\frac{[\lambda-\lambda_{\mathrm{peak\_g}}(P_d,T_j)]^2}{\sigma_g(T_j)^2}\right\} + \eta_y(T_j)P_{\mathrm{opt\_total}}(P_d,T_j)\frac{1}{\sigma_y\sqrt{2\pi}} \times \exp\left\{-0.5^*\frac{[\lambda-\lambda_{\mathrm{peak\_y}}(P_d,T_j)]^2}{\sigma_y(T_j)^2}\right\}. \quad (14)$$

B. Time Dependence of the Junction Temperature

Based on the dynamic PET theory [16], the thermal transient characteristics of the junction temperature for the LED mounted on a heat sink can be expressed as

$$T_j(t) = \begin{bmatrix} -R_{jc}k_hP_d\left(\frac{C_{jc}NR_{hs}}{C_{jc}R_{jc}-C_{hs}R_{hs}}+1\right)e^{-\frac{t}{C_{jc}R_{jc}}} \\ +k_hP_d\frac{NR_{hs}^2C_{hs}}{C_{jc}R_{jc}-C_{hs}R_{hs}}e^{-\frac{t}{C_{hs}R_{hs}}} \\ +(R_{jc}+NR_{hs})\,k_hP_d+T_0 \end{bmatrix} \quad (15)$$

where R_{jc} and C_{jc} are the thermal resistance and thermal capacitance of the LED package, respectively; R_{hs} and C_{hs} are the heat sink's thermal resistance and thermal capacitance, respectively; and N is the number of LED. The thermal resistance and thermal capacitance for different materials along the heat flow path can be extracted from Fig. 7, which indicates the cumulative structure function based on the thermal transient test method [17], [20]. The thermal resistance of the adhesive layer is usually smaller than R_{jc} and can be included in R_{jc} if necessary for simplicity. Based on the measured results, the parameters required for (15) are included in Table V.

IV. EXPERIMENTAL VERIFICATIONS

Two different types of LED devices were used to evaluate the validity and accuracy of the electro-thermo-temporal SPD modeling. The optical measurements of the LED samples were measured in thermal and electrical steady-state conditions using the TeraLED system. To establish the dependence of the wall-plug efficiency on the LED electrical power, the LED sample was operated in the pulsewidth of 300 μs and duty cycle of 0.03% in order to eliminate the Joule heating dependence on the efficiency. Immediately after all optical measurements, the LED was switched off, and the cooling transient of the LED package was monitored with the use of the Transient Thermal Tester (T3Ster).

Aside from the combined thermal and optical measurements, the temperature dependence of the optical power and the wall-plug efficiency of the LED were also recorded. The theoretical framework of the evaluation of the T3Ster was based on the distribution RC networks [20]. The T3Ster captured the thermal transient response in real time, recorded the cooling/heating curve, and then evaluated the cooling/heating curve so as to derive the thermal characteristics [17]. The diode voltage is temperature dependent. For the voltage–temperature sensitive

TABLE IV
EXTRACTED PARAMETERS FOR (13) BASED ON MEASUREMENTS

	α	β	χ	δ	γ	μ
Sharp 4.4W	-0.000270	0.206	0.00148	-0.0252	0.256	0.188
Sharp 8W	-0.000522	0.270	0.00088	-0.0175	0.275	0.229

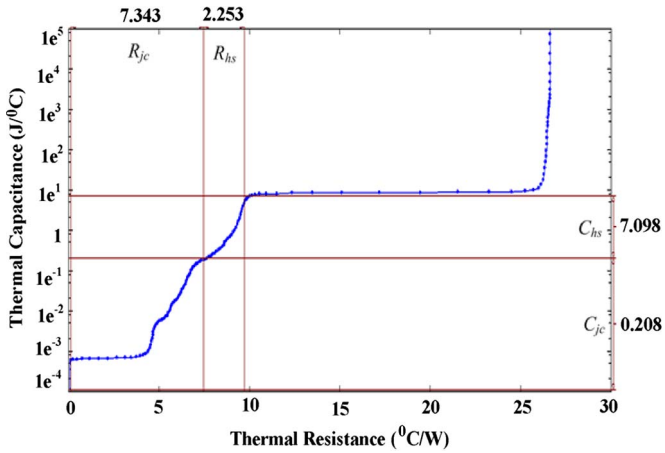

Fig. 7. Cumulative structure function for Sharp 4.4-W LED.

parameter calibration, a 5-mA current was applied in the temperature range of 25 °C–55 °C with an increment of 10 °C. Then, the junction temperature values were captured using the voltage response curve and the voltage–temperature sensitivity calibration.

The light output and transient thermal curves were measured after driving the LED with a current for 20 min with the heat sink temperature kept constant. The steady-state radiation power spectra of the samples were captured with the use of a PMS-50 spectrophotocolorimeter with an integrating sphere after 20 min of operation at different electrical power at an ambient temperature of 20 °C. The optical power for the blue emission spectra and the phosphor emission spectra can be calculated by integrating the photon energy corresponding to blue and phosphor wavelength.

The transient color characteristic of the samples was captured with the use of the Konica Minolta Spectroradiometer CS-2000, which had a bandwidth of 0.1 Hz. However, this instrument could measure light from a limited area of the LED at a particular angle. The measured color result represented only the partial color properties of LED at this view angle. (Note that the color properties were affected by different phosphor thicknesses, concentrations, and particle sizes on LED chip surface and the view angle.) In order to calibrate the color measurements with the SPD measurements, the steady-state spectra of the samples were captured with the integrating sphere associated with the PMS-50 spectrophotocolorimeter, which can evaluate the color properties from all view angles.

A key emphasis on the proposed method is that, based on the steady-steady measurements obtainable from lighting equipment with limited bandwidth, the spectral modeling approach can be applied not only to steady-state modeling but also to dynamic modeling using the framework of the dynamic PET theory. This advantage is now illustrated with some practical examples.

A. Test on Sharp 4.4-W LED (Model Number: GW5BNC15L02)

1) Steady-State Measurement: Putting the related parameters of the Sharp 4.4-W LED sample in Tables I–IV into (14), the theoretical SPD modeling with electrical power and junction temperature can be established for this LED sample. The values of the chromaticity coordinates are measured at different electrical power in Fig. 8. Based on the electrothermal SPD modeling, the theoretical values of the chromaticity coordinate obtained at the same electrical power from (14) are shown in Fig. 9. The CCT and CRI of the samples are measured and calculated as shown in Figs. 10 and 11, respectively. The measured and theoretical results show good agreement, which confirms the accuracy of the proposed modeling method, at least for the steady-state color characteristics. It is noted that the CCT moves toward to cooler CCT with increasing electrical power due to the temperature dependence of the peak wavelength, FWHM, and $P_{\mathrm{opt\_phosphor}}/P_{\mathrm{opt\_b}}$. The measured and calculated chromaticity coordinates (x,y) for the Sharp 4.4-W LED initially increase as the electrical power P_d increases (due to the piezoelectricity-induced quantum-confined Stark effect). As P_d continues to increase, the chromaticity coordinates begin to decrease (due to the domination of bandgap energy with temperature). The variations in chromaticity coordinates due to electrical and thermal stress changes can also be represented by the shift of CCT and CRI. The variations of the CCT and CRI with electrical power also show parabolic relationships. The procedure for the required steps for the steady-state measurements is provided in Flow Chart 1.

2) Dynamic Measurements: In order to check the dynamic performance of the electro-thermal-temporal SPD modeling, the LED sample is driven with a varying current with a ripple of 0.1 Hz by a programmable power source. The frequency of the current ripple is set at 0.1 Hz because of the limitation in the bandwidth of the Konica Minolta Spectroradiometer CS-2000. The Sharp 4.4-W LED is mounted on a heat sink with thermal resistance R_{hs} of 2.253 °C/W and thermal capacitance C_{hs} of 7.097 J/°C. The instantaneous power and current waveforms are captured in Fig. 12. The maximum and minimum LED power values are 4.16 and 0.68 W, respectively. For the transient thermal characteristics of the LED, the related parameters are listed in Table V. They are used in (15) for the calculation of the junction temperature as a function of time (see Fig. 13). Putting this dynamic junction temperature in (14), the electro-thermal-temporal SPD can be established. The dynamic variations of CCT and CRI can be theoretically determined. The measured and calculated values of the chromaticity coordinates are shown in Fig. 14, while those of the CCT are shown in Fig. 15. The coefficient of determination R^2 method is used to check the agreement of the measured and calculated results. The coefficients of determination for Figs. 14 and 15 are 0.921 and 0.761, respectively (with a figure of 1.0 for a perfect match).

TABLE V
EXTRACTED PARAMETERS FOR (15) BASED ON MEASUREMENTS

	k_h	T_a(℃)	R_{jc}(℃/W)	C_{jc}(J/℃)	R_{hs}(℃/W)	C_{hs}(J/℃)	N
Sharp 4.4W	0.78	20	7.343	0.208	2.253	7.097	1
Sharp 8W	0.75	20	5.216	0.212	2.479	6.003	1

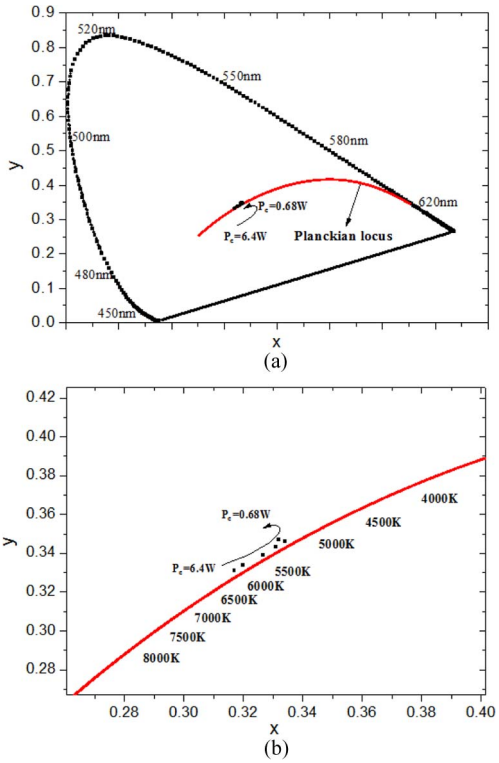

Fig. 8. Measured chromaticity coordinates of Sharp 4.4-W LED for different electrical power. (a) Measured chromaticity coordinates. (b) Expanded view.

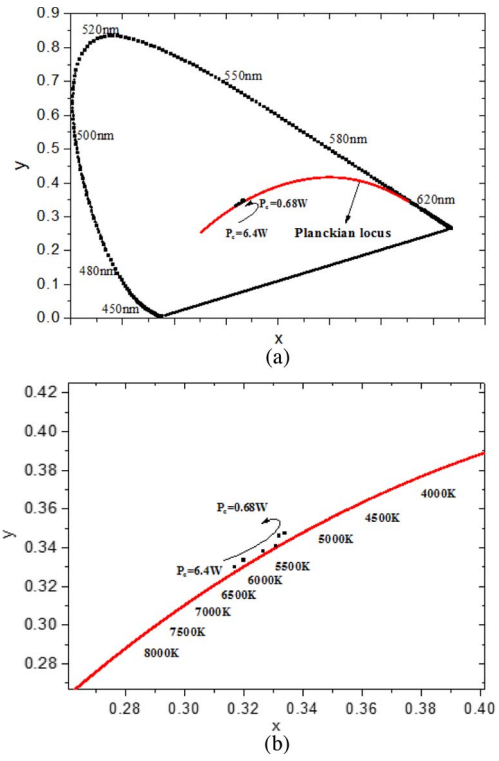

Fig. 9. Calculated chromaticity coordinates of Sharp 4.4-W LED for different electrical power. (a) Calculated chromaticity coordinates. (b) Expanded view.

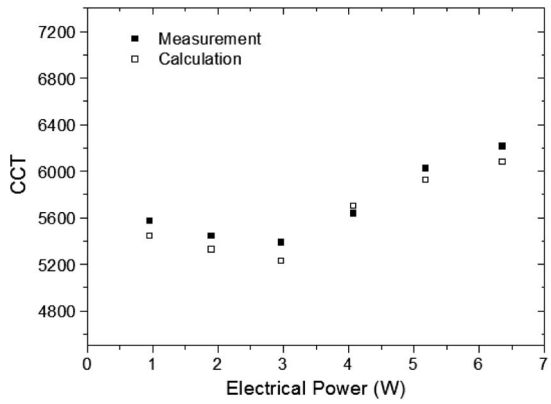

Fig. 10. Measured and calculated CCTs of Sharp 4.4-W LED for a range of electrical power.

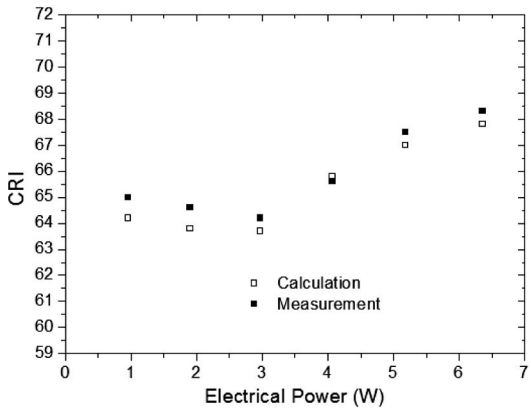

Fig. 11. Measured and calculated CRIs of Sharp 4.4-W LED for a range of electrical power.

It is noted that the calculated results are generally consistent with practical measurements. Their good agreements confirm the accuracy of the proposed modeling method for dynamic measurements.

With the dynamic prediction of CCT and CRI confirmed, the SPD model can be used with the dynamic PET theory, which includes the thermal time constants of both of the LED packages and the heat sinks in (15), to predict the dynamic variation of the CCT at other frequencies. The predicted junction temperature and CCT at several time intervals (from 1 s to 20 min of continuous operation) from the beginning of the test are plotted in Figs. 16 and 17, respectively. Such information allows application designers to predict the LED performance before finalizing their designs.

B. Test on Sharp 8-W LED (Model Number: GW5BWF15L00)

1) Steady-State Measurement: The same series of tests are then repeated using the Sharp 8-W LED sample. Putting the parameters of the Sharp 8-W LED in Tables I–IV into (14), the theoretical SPD modeling with electrical power and junction

FLOW CHART 1: PROCEDURE OF THE MODELING METHOD (ASSUMING THAT THE RELEVANT SPECTRAL INFORMATION IS NOT AVAILABLE FROM THE DATA SHEET)

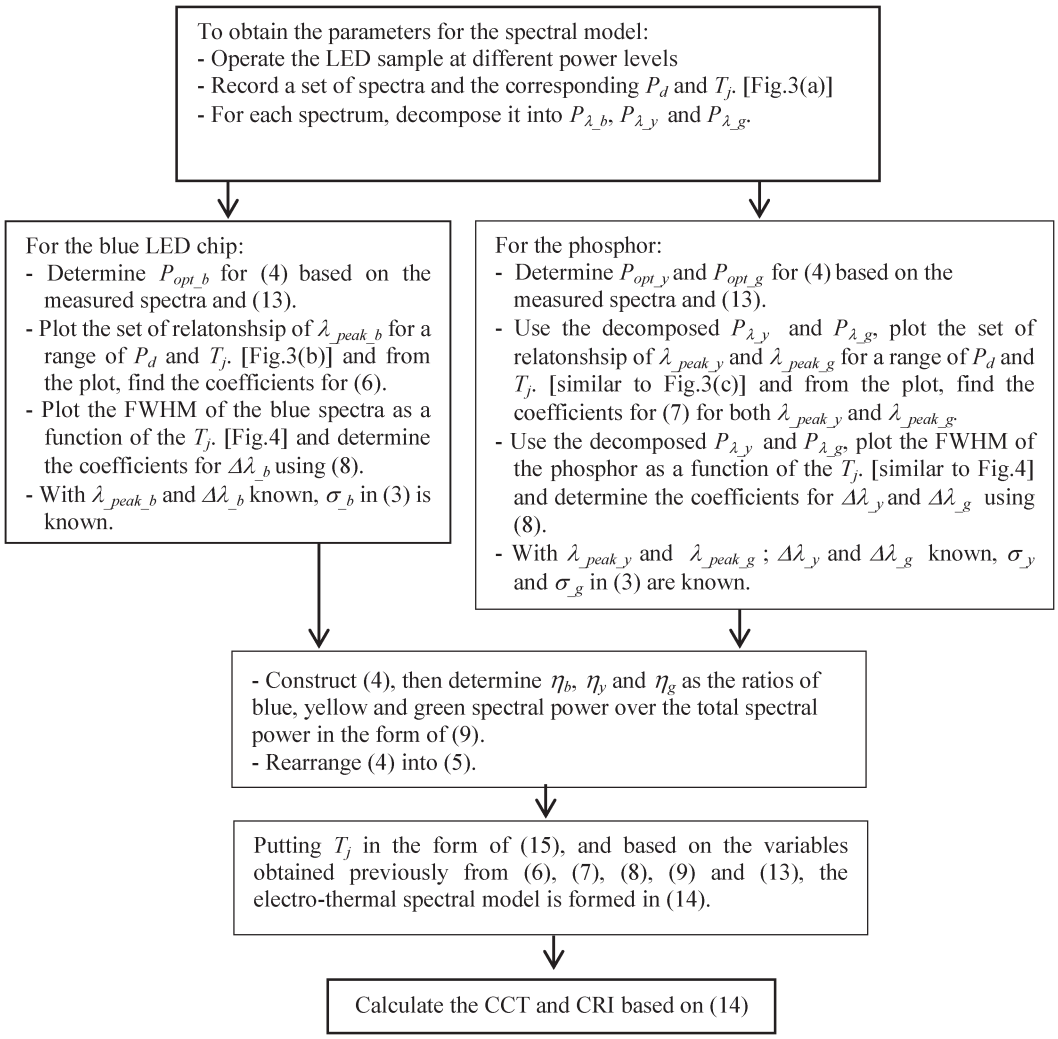

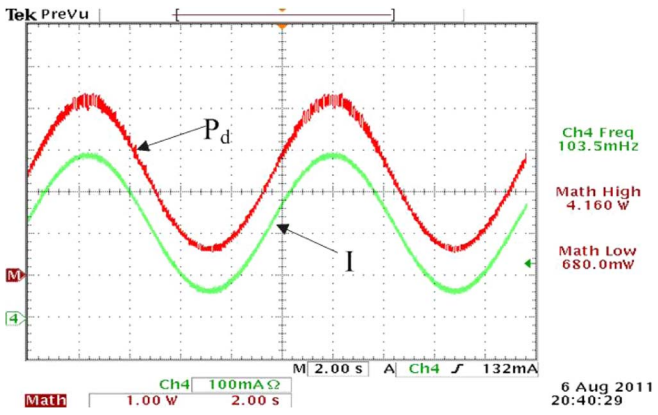

Fig. 12. Measured power and current of the Sharp 4.4-W LED driven at 0.1 Hz under thermal equilibrium.

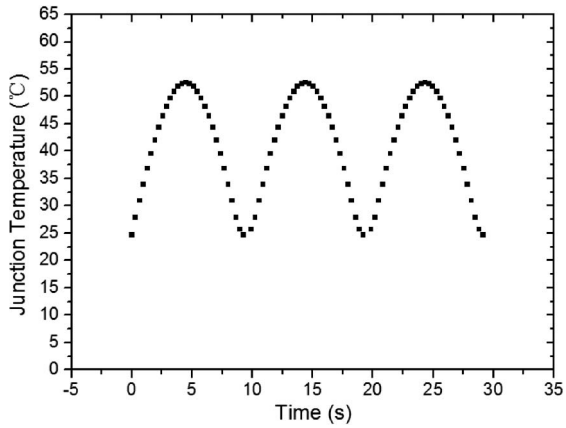

Fig. 13. Junction temperature of the Sharp 4.4-W LED driven at 0.1 Hz under thermal equilibrium.

temperature can be established. The measured values of the chromaticity coordinates are recorded at different electrical power and shown in Fig. 18. Based on the electrothermal SPD modeling, the theoretical values of the chromaticity coordinates obtained at the same electrical power from (14) are shown in Fig. 19. The results of the CCT and CRI of the LED sample are plotted in Figs. 20 and 21, respectively. Good agreements between the theoretical calculations and practical measurements confirm the validity of the proposal method.

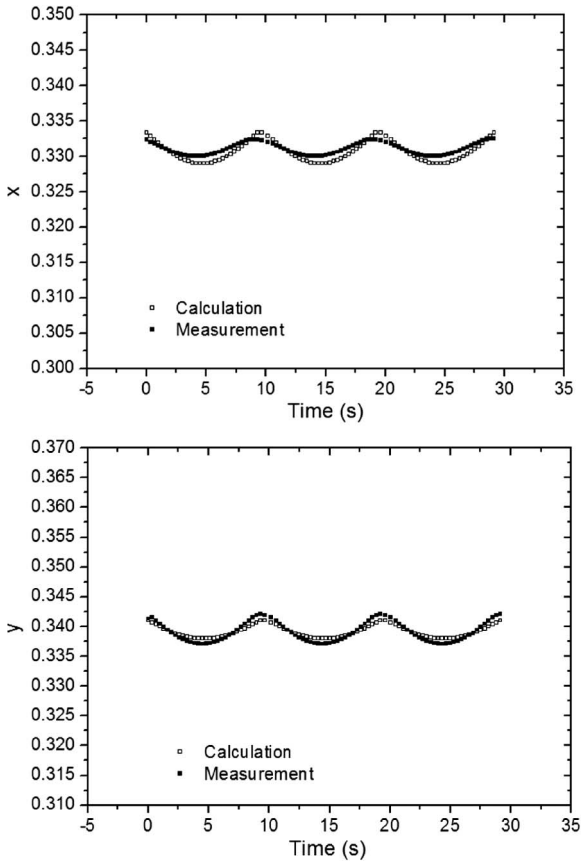

Fig. 14. Measured and calculated chromaticity values for Sharp 4.4-W LED driven at 0.1 Hz under thermal equilibrium.

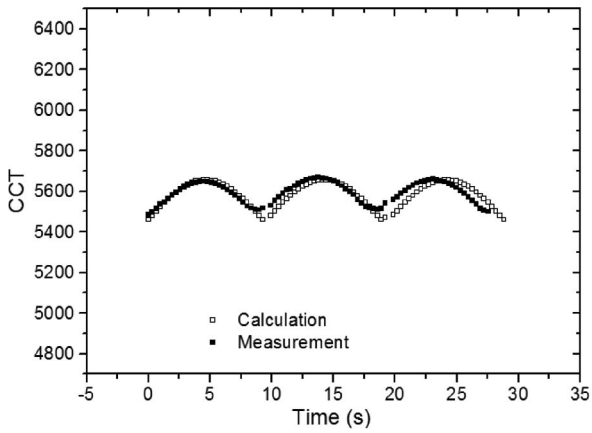

Fig. 15. Measured and calculated CCTs for Sharp 4.4-W LED driven at 0.1 Hz under thermal equilibrium.

2) Dynamic Measurements: Mounted on a heat sink with a thermal resistance of 2.48 °C/W and a thermal capacitance of 6.00 J/°C, the Sharp 8-W sample is excited with a current with a ripple of 0.1 Hz as in the previous dynamic tests. The instantaneous power and current waveforms are shown in Fig. 22. The parameters for the transient thermal characteristics of the LED are listed in Table V.

The variation of the junction temperature calculated with (15) is plotted in Fig. 23. Putting the junction temperature

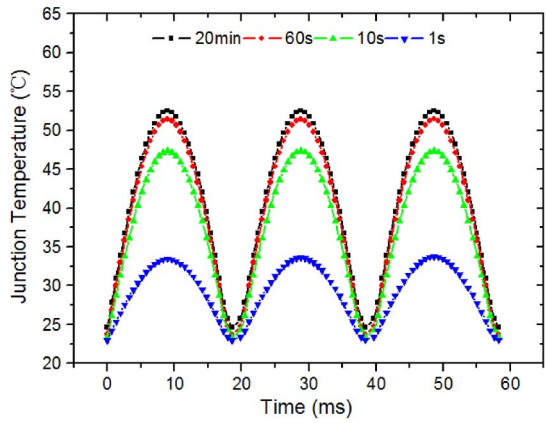

Fig. 16. Calculated junction temperature of the Sharp 4.4-W LED after different periods of continuous operation.

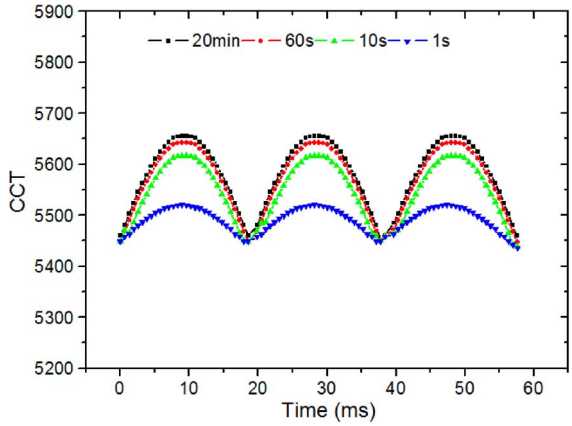

Fig. 17. Calculated CCT of the Sharp 4.4-W LED after different periods of continuous operation.

response in Fig. 23 into (14), the electro-thermal-temporal SPD modeling can be established. The calculated and measured values of the chromaticity coordinates are shown in Fig. 24, and those of CCT are shown in Fig. 25 for a range of power. The coefficient of determination R^2 is used in the measured and calculated results to check the agreement between data sets. The coefficients of determination for Figs. 24 and 25 are 0.901 and 0.713, respectively. The good agreements of the measured and the calculated CCT in these dynamic tests confirm the accuracy of the proposed theory, which can be used as a design tool for the prediction of junction temperature and CCT even over a long period of time as shown in Fig. 25.

Equation (15) is then used to generate the junction temperature response for an operating frequency of 50 Hz of input power. The responses of the junction temperature and CCT are recorded at several time intervals (from 1 s to 20 min) from the beginning of the test and plotted in Figs. 26 and 27. It can be seen that the maximum junction temperature and CCT increase from about 32.5 °C and 5302 K (measured 1 s after initial operation) to about 46.5 °C and 5454 K (measured 20 min later). The CCT increases by 152 K. The CCT increases with time because the junction temperature of the device increases gradually with time.

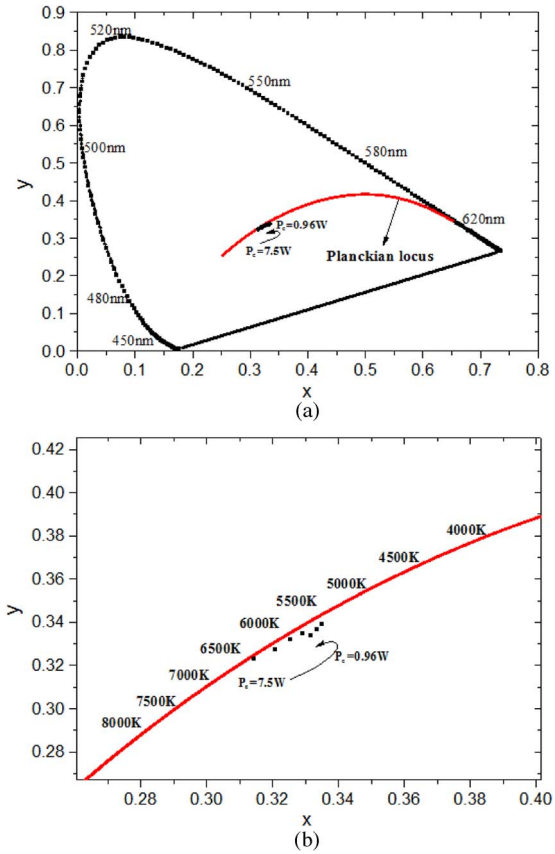

Fig. 18. Measured chromaticity coordinates of Sharp 8-W LED for different electrical power. (a) Measured chromaticity coordinates. (b) Expanded view.

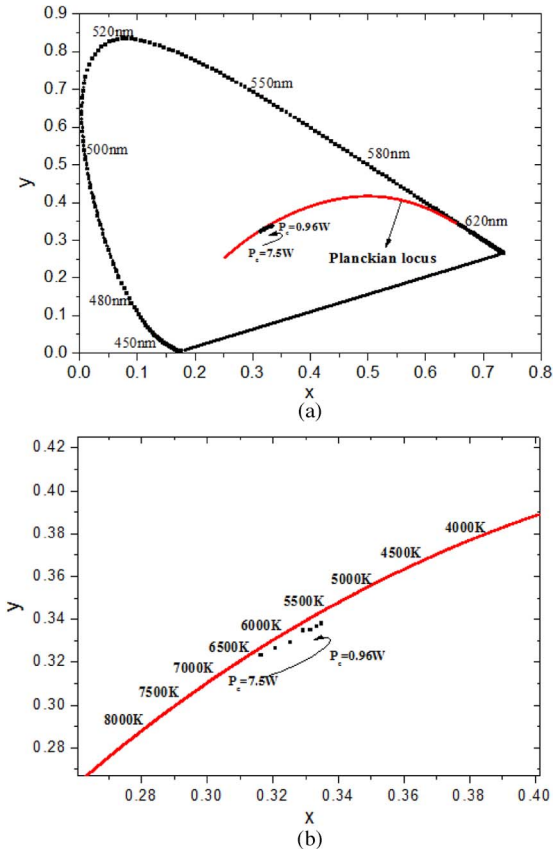

Fig. 19. Calculated chromaticity coordinates of Sharp 8-W LED for different electrical power. (a) Calculated chromaticity coordinates. (b) Expanded view.

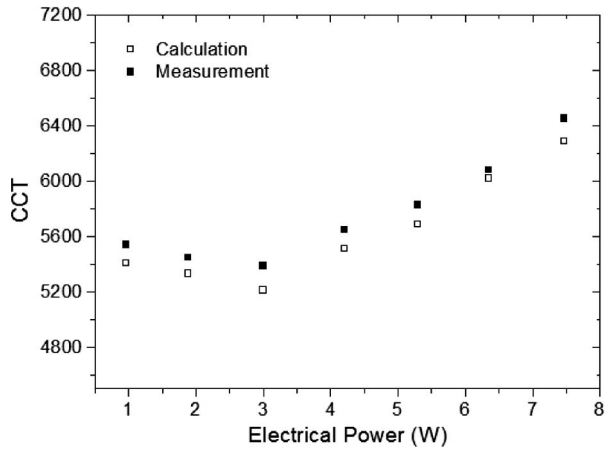

Fig. 20. Measured and calculated CCTs of Sharp 8-W LED for different electrical power.

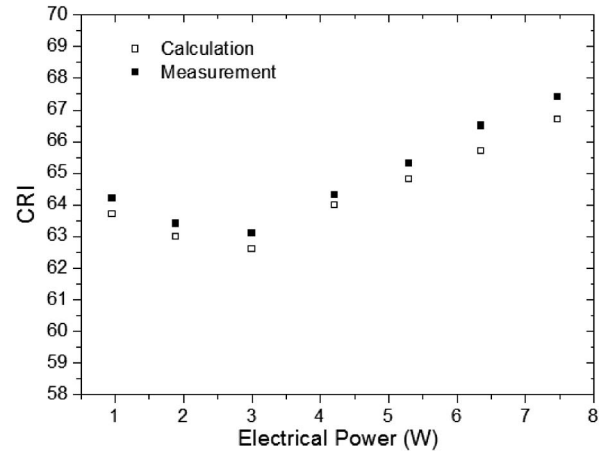

Fig. 21. Measured and calculated CRIs of Sharp 8-W LED for different electrical power.

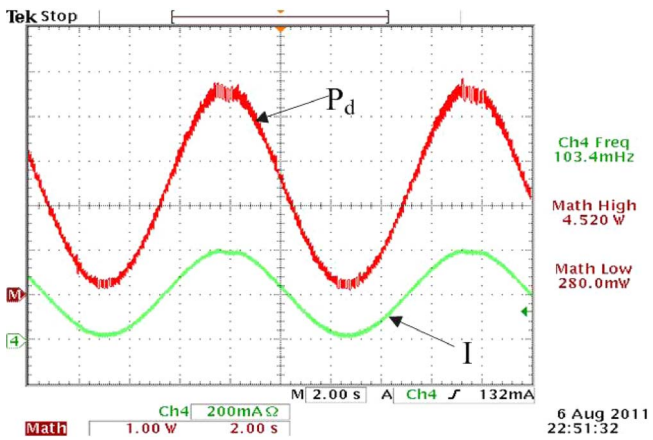

Fig. 22. Measured power and current of the Sharp 8-W LED driven at 0.1 Hz under thermal equilibrium.

C. Use of the Spectral Model as a Dynamic Modeling Tool

With the confirmation that the spectral model can be applied for dynamic prediction, the spectral model can be employed for studying the variations of chromatic aspects of LED lighting applications such as the effects of dimming on the CCT. Fig. 28(a) shows a dimming action for the 8-W LED sample changing from about 7.5 to 1 W over a transitional time of 2 s.

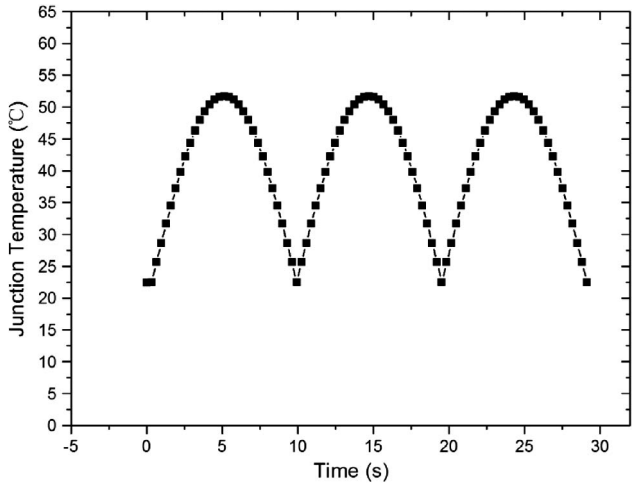

Fig. 23. Junction temperature response for Sharp 8-W LED driven at 0.1 Hz under thermal equilibrium.

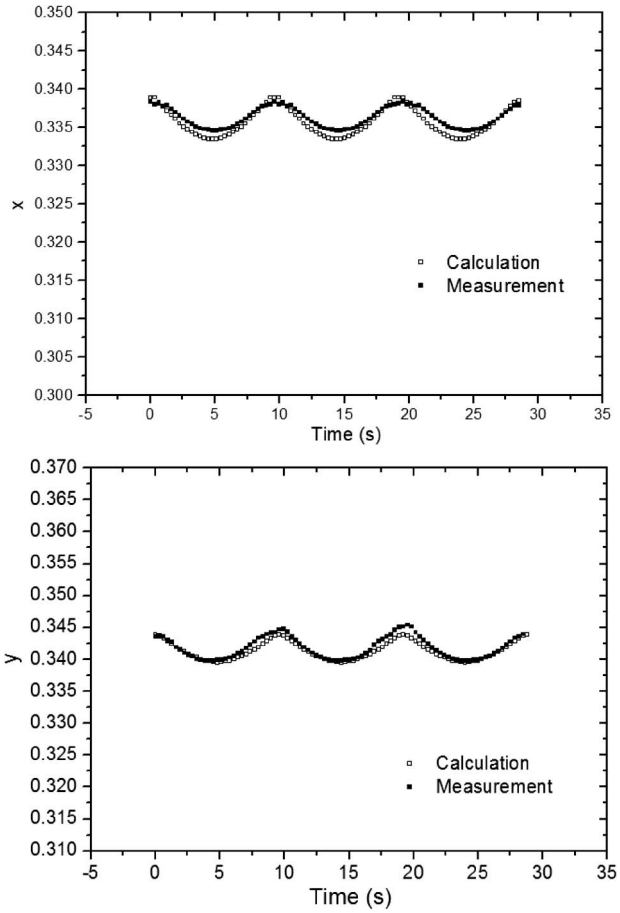

Fig. 24. Measured and calculated chromaticity coordinates of the Sharp 8-W LED driven at 0.1 Hz under thermal equilibrium.

The dynamic curve of the CCT is plotted in Fig. 28(b). The predicted CCT changes quickly from about 6450 K to about 6150 K immediately after the power change and then gradually from 6150 K to about 5550 K. The reason for the two rates of change of the CCT can be explained by the fact that the thermal time constant of the LED package $(R_{jc}C_{jc})$ is much smaller than that of the heat sink $(R_{hs}C_{hs})$. This dynamic modeling shows that the steady-state CCT change of 900 K

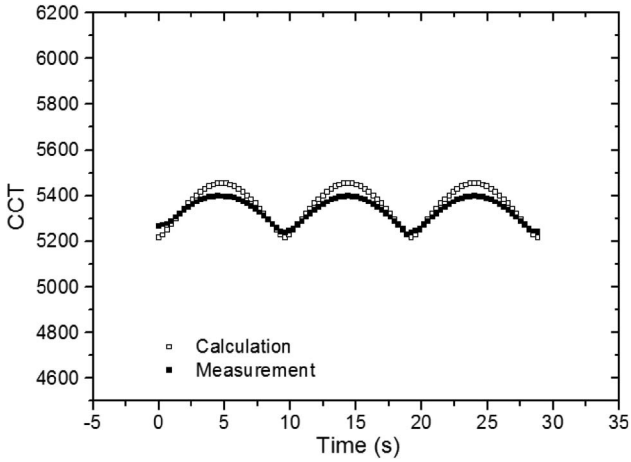

Fig. 25. Measured and calculated CCTs of the Sharp 8-W LED driven at 0.1 Hz under thermal equilibrium.

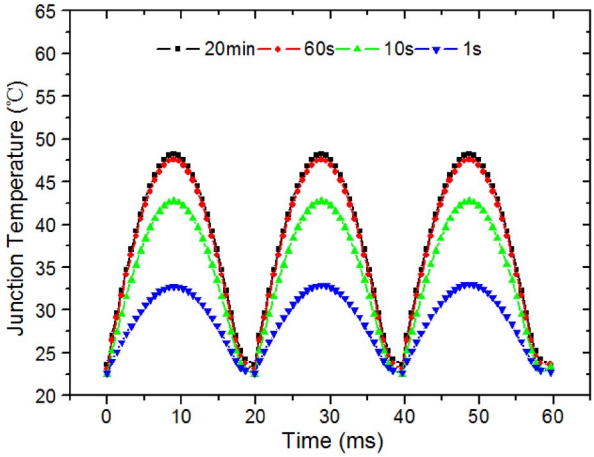

Fig. 26. Calculated junction temperature of the Sharp 8-W LED after different periods of continuous operation.

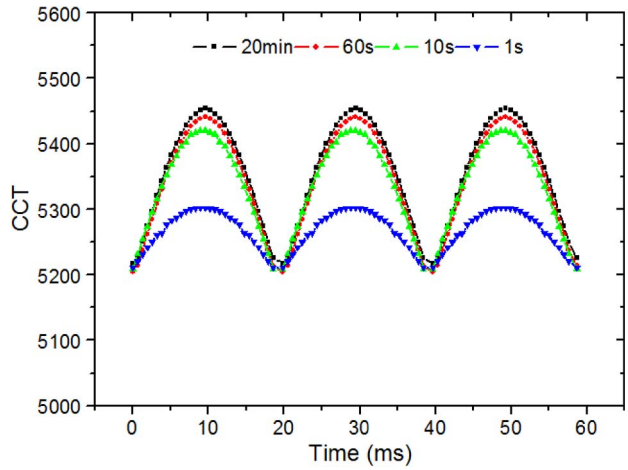

Fig. 27. Calculated CCT of the Sharp 8-W LED after different periods of continuous operation.

is much worse than the initial CCT change of 300 K observed immediately after the dimming action. While such fast dynamic CCT changes cannot be captured with lighting equipment with limited bandwidth, they can now be studied in simulations using the proposed method.

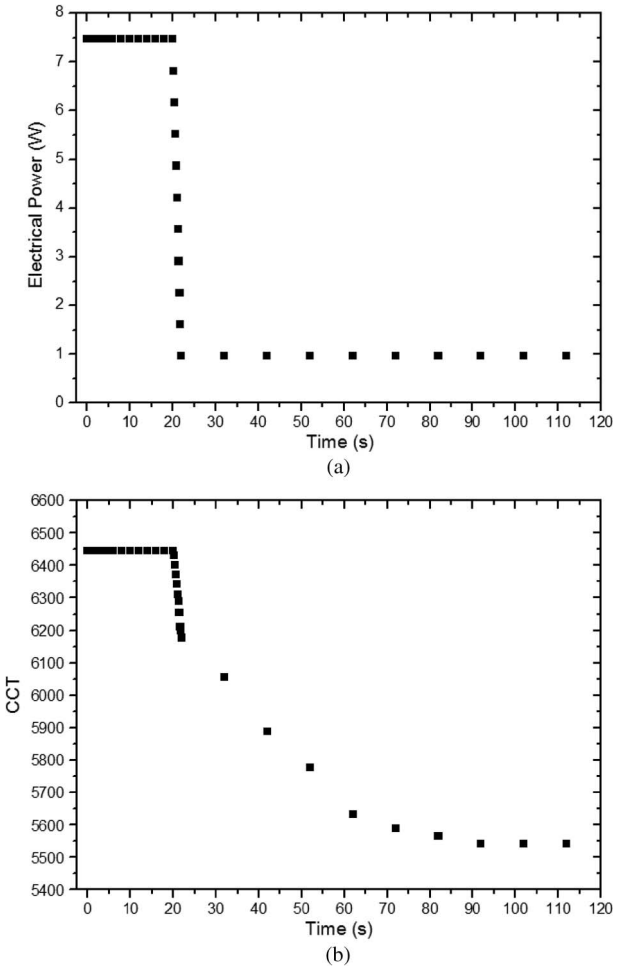

Fig. 28. (a) Step change of power for an 8-W LED over a 2-s transitional time (dimming action). (b) Predicted dynamic variation of the CCT with time.

V. Conclusion

A tricolor spectral modeling method has been developed for the SPDs of white LED based on blue LED and yellow phosphor. Such modeling method has been incorporated into the framework of the steady-state and dynamic PET theory so that chromatic variables such as CCT and CRI can be predicted with the LED devices in a system environment, including the effects of the LED package, heat sink, and LED power varied by a LED driver. The proposed spectral model links the junction temperature, electrical power, and time variable together. It has been favorably confirmed with chromatic measurements of two types of LED devices. It is envisaged that this is the first theoretical tool for predicting color properties of phosphor-coated white LED systems. The lack of an international standard on the binning systems of LEDs has somehow restricted the widespread applications of LED lighting in certain general lighting applications. It is suggested that LED manufacturers should consider including the spectral modeling parameters in the data sheets so that this theoretical tool can be used by researchers/design engineers to devise new techniques [25]–[27] in designing or controlling CCT and CRI in future LED systems.

References

[1] W. Davis and Y. Ohno, "Toward an improved color rendering metric," in *Proc. SPIE*, 2005, vol. 5941, pp. 59411G1–59411G8.
[2] W. Davis and Y. Ohno, "Color quality scale," *Opt. Eng.*, vol. 49, no. 3, pp. 033602–033616, Mar. 2010.
[3] S. C. Tan, "General n-level driving approach for improving electrical-to-optical energy-conversion efficiency of fast-response saturable lighting devices," *IEEE Trans. Ind. Electron.*, vol. 57, no. 4, pp. 1342–1353, Apr. 2010.
[4] K. H. Loo, Y. M. Lai, S. C. Tan, and C. K. Tse, "Stationary and adaptive color-shift reduction methods based on the bilevel driving technique for phosphor-converted white LEDs," *IEEE Trans. Power Electron.*, vol. 26, no. 7, pp. 1943–1953, Jul. 2011.
[5] K. H. Loo, Y. M. Lai, S. C. Tan, and C. K. Tse, "On the color stability of phosphor-converted white LEDs under dc, PWM, and bilevel drive," *IEEE Trans. Power Electron.*, vol. 27, no. 2, pp. 974–984, Feb. 2012.
[6] S. Chhajed, Y. Xi, Y. L. Li, T. Gessmann, and E. F. Schubert, "Influence of junction temperature on chromaticity and color-rendering properties of trichromatic white-light sources based on light-emitting diodes," *J. Appl. Phys.*, vol. 97, no. 5, pp. 054506-1–054506-8, Mar. 2005.
[7] A. Keppens, W. R. Ryckaert, G. Deconinck, and P. Hanselaer, "Modeling high power light-emitting diode spectra and their variation with junction temperature," *J. Appl. Phys.*, vol. 108, no. 4, pp. 043104-1–043104-7, Aug. 2010.
[8] S. Choi and T. Kim, "Symmetric current-balancing circuit for LED backlight with dimming," *IEEE Trans. Ind. Electron.*, vol. 59, no. 4, pp. 1698–1707, Apr. 2012.
[9] F. Reifegerste and J. Lienig, "Modeling of the temperature and current dependence of LED spectra," *J. Light Vis. Environ.*, vol. 32, no. 3, pp. 288–294, 2008.
[10] Y. Uchida and T. Taguchi, "Light theory and luminous characteristics of white light-emitting diodes," *Opt. Eng.*, vol. 44, no. 12, pp. 124003-1–124003-19, Dec. 2005.
[11] Y. Ohno, "Spectral design considerations for white LED color rendering," *Opt. Eng.*, vol. 44, no. 11, pp. 111302-1–111302-9, Nov. 2005.
[12] K. Man and I. Ashdown, "Accurate colorimetric feedback for RGB LED clusters," in *Proc. SPIE*, Aug. 2006, vol. 6337, pp. 633702-1–633702-8.
[13] H. Y. Chou and T. H. Yang, "Dependence of emission spectra of LEDs upon junction temperature and driving current," *J. Light Vis. Environ.*, vol. 32, no. 2, pp. 183–187, 2008.
[14] S. Y. R. Hui and Y. X. Qin, "A general photo-electro-thermal theory for light-emitting-diode (LED) systems," *IEEE Trans. Power Electron.*, vol. 24, no. 8, pp. 1967–1976, Aug. 2009.
[15] S. Y. R. Hui, H. T. Chen, and X. H. Tao, "An extended photoelectrothermal theory for LED systems: A tutorial from device characteristic to system design for general lighting," *IEEE Trans. Power Electron.*, vol. 27, no. 11, pp. 4571–4583, Nov. 2012.
[16] X. H. Tao and S. Y. R. Hui, "Dynamic photoelectrothermal theory for LED systems," *IEEE Trans. Ind. Electron.*, vol. 59, no. 4, pp. 1751–1759, Apr. 2012.
[17] A. Poppe, G. Farkas, V. Székely, G. Horváth, and M. Rencz, "Multi-domain simulation and measurement of power LED-s and power LED assemblies," in *Proc. 22nd IEEE SEMI-THERM*, Dallas, TX, USA, Mar. 2006, pp. 191–198.
[18] Y. Gu and N. Narendran, "A non-contact method for determining junction temperature of phosphor-converted white LEDs," in *Proc. SPIE*, Jan. 2004, vol. 5187, pp. 107–114.
[19] H. T. Chen, X. H. Tao, and S. Y. R. Hui, "Estimation of optical power and heat dissipation coefficient for the photo-electro-thermal theory for LED systems," *IEEE Trans. Power Electron.*, vol. 27, no. 4, pp. 2176–2183, Apr. 2012.
[20] G. Farkas, Q. V. V. Vader, A. Poppe, and G. Bognár, "Thermal investigation of high power optical devices by transient testing," *IEEE Trans. Compon., Packag., Manuf. Technol.*, vol. 28, no. 1, pp. 45–50, Mar. 2005.
[21] V. P. Varshni, "Temperature dependence of the energy gap in semiconductors," *Physica*, vol. 34, no. 1, pp. 149–154, Apr. 1967.
[22] D. S. Peng and K. Jin, "The influence of driving current on emission spectra of GaN-based LED," in *Proc. ICEOE*, Jul. 2011, vol. 2, pp. V2-148–V2-151.
[23] E. F. Schubert, *Light Emitting Diodes,* 2nd ed. Cambridge, U.K.: Cambridge Univ. Press, 2006, p. 106.
[24] I. Baginskiy, R. S. Liu, C. L. Wang, R. T. Lin, and Y. J. Yao, "Temperature dependent emission of strontium-barium orthosilicate (Sr 2-xBax)SiO4: Eu2+ phosphors for high-power white light-emitting diodes," *J. Electrochem. Soc.*, vol. 158, no. 10, pp. P118–P121, 2011.

[25] S. K. Ng, K. H. Loo, S. K. Ip, Y. M. Lai, C. K. Tse, and K. T. Mok, "Sequential variable bilevel driving approach suitable for use in high-color-precision LED display panels," *IEEE Trans. Ind. Electron.*, vol. 59, no. 12, pp. 4637–4645, Dec. 2012.
[26] J. M. Zhang, J. F. Wang, and X. K. Wu, "A capacitor-isolated LED driver with inherent current capability," *IEEE Trans. Ind. Electron.*, vol. 59, no. 4, pp. 1708–1716, Apr. 2012.
[27] R. A. Pinto, M. R. Cosetin, A. Campos, M. A. C. Dalla, and R. N. D. Prado, "Compact emergency lamp using power LEDs," *IEEE Trans. Ind. Electron.*, vol. 59, no. 4, pp. 1728–1738, Apr. 2012.

Huanting Chen received the Ph.D. degree in radio physics from Xiamen University, Xiamen, China, in 2010.

He was a Lecturer with Zhangzhou Normal University, Zhangzhou, China. He is currently a Research Associate with the Department of Electrical and Electronic Engineering, The University of Hong Kong, Hong Kong. His research interests include solid-state lighting technology and applications.

S. Y. (Ron) Hui (M'87–SM'94–F'03) received the B.Sc.(Hons.) degree in engineering from the University of Birmingham, Birmingham, U.K., in 1984 and the D.I.C. and Ph.D. degrees from Imperial College London, London, U.K., in 1987.

He has previously held academic positions at the University of Nottingham, Nottingham, U.K. (1987–1990), the University of Technology, Sydney, Australia (1990–1991), the University of Sydney, Sydney (1992–1996), and the City University of Hong Kong, Kowloon, Hong Kong (1996–2011). Currently, he is the holder of the Philip Wong Wilson Wong Chair Professorship at The University of Hong Kong, Hong Kong. Since July 2010, he has concurrently held the Chair Professorship of Power Electronics at Imperial College London. He has published over 270 technical papers, including more than 160 refereed journal publications and book chapters. More than 55 of his patents have been adopted by industry.

Prof. Hui is a Fellow of the Institution of Engineering and Technology, U.K. He has been an Associate Editor of the IEEE TRANSACTIONS ON POWER ELECTRONICS since 1997 and an Associate Editor of the IEEE TRANSACTIONS ON INDUSTRIAL ELECTRONICS since 2007. He was appointed twice as an IEEE Distinguished Lecturer by the IEEE Power Electronics Society in 2004 and 2006. He served as one of the 18 Administrative Committee members of the IEEE Power Electronics Society and was the Chairman of its Constitution and Bylaws Committee from 2002 to 2010. He received the Teaching Excellence Award in 1998 and the Earth Champion Award in 2008. He won an IEEE Best Paper Award from the IEEE Industry Applications Society Committee on Production and Application of Light in 2002 and two IEEE Power Electronics Transactions Prize Paper Awards for his publications on Wireless Charging Platform Technology in 2009 and on LED System Theory in 2010. His inventions on wireless charging platform technology underpin key dimensions of Qi, the world's first wireless power standard, with freedom of positioning and localized charging features for wireless charging of consumer electronics. He is a coinventor of electric springs. He was the recipient of the IEEE Rudolf Chope R&D Award from the IEEE Industrial Electronics Society in November 2010 and the IET Achievement Medal (The Crompton Medal) and was elected to Fellowship of the Australian Academy of Technological Sciences and Engineering.